Nanostructured Assemblies for Dental Application

Florence Fioretti,[†,§,#] Carlos Mendoza-Palomares,[†,§,#] Marie Helms,[†,§] Denise Al Alam,[⊥] Ludovic Richert,[¶] Youri Arntz,[¶] Simon Rinckenbach,[†] Fabien Garnier,[‖] Youssef Haïkel,[†,§] Sophie C. Gangloff,[⊥,*] and Nadia Benkirane-Jessel[†,‡,*]

[†]Institut National de la Santé et de la Recherche Médicale (INSERM), Unité 977, 11 rue Humann, Strasbourg, France, [‡]Hôpital Central, Service de Chirurgie Orthopédique and CNRS UMR 7561, 29, Av. du Maréchal de Lattre de Tassigny, 54035 Nancy Cedex, France, [§]Faculté de Chirurgie Dentaire, Université de Strasbourg, UdS. Strasbourg, France, [⊥]Laboratoire Immuno-Pharmacologie Cellulaire et Moléculaire, EA3796 UFR Pharmacie, URCA, 51, Rue Cognacq Jay, Reims, France, [‖]IBMM, UMR 5247, CNRS, Universite Montpellier 1&2, present address COLCOM, Cap Alpha, Avenue de l' Europe,Clapiers, 34940 Montpellier Cedex 9, France, and [¶]Centre National de la Recherche Scientifique (CNRS) UMR 7213, Faculté de Pharmacie de l'Université de Strasbourg (UdS), 74, route du Rhin, 67401 Illkirch Cedex, France. [#]These authors contributed equally to this work.

I n teeth with periradicular lesions, the removal of the irritants (inflamed or necrotic tissue) from the root canal system begins the process of repair and resolution. Repair of periradicular lesions is primarily characterized by inflammatory cell infiltration, which is responsible for removal of endogenous and exogenous irritants, followed by fibroblastic proliferation collagen deposition, bone formation, and cement apposition when root desorption occurs.

Most periapical diseases are induced as a result of direct or indirect involvement of oral bacteria. In most cases, the etiological factors are oral contaminants through the root canal or degenerating pulpal tissues. Because bacteria initiate and perpetuate the pulpal tissues, we need to control not only bacterial progression in pulpal and periapical diseases but also the responses of pulpal and periapical tissues to bacterial infection. The control of the pulp fibroblast response is fundamental to control the pulp inflammation. To control the pulp inflammation after infection, the aim of this study was to investigate the anti-inflammatory effects of a biologically active film on human pulp fibroblasts by using the melanocortin peptides (α-MSH) as active molecule.[1]

Melanocortin peptides (α-MSH) are crucial in cutaneous biology,[2] but also involved in other tissue metabolism as adipose tissue and bone,[3,4] α-MSH has been shown to possess anti-inflammatory effects in many experimental models of acute and chronic inflammation.[5−7] α-MSH is also able to reduce tissue fibrosis.[8] To date, five melanocortin receptors (MCR) coupled to adenylate cyclase have been identified based on their

ABSTRACT Millions of teeth are saved each year by root canal therapy. Although current treatment modalities offer high levels of success for many conditions, an ideal form of therapy might consist of regenerative approaches in which diseased or necrotic pulp tissues are removed and replaced with healthy pulp tissue to revitalize teeth. Melanocortin peptides (α-MSH) possess anti-inflammatory properties in many acute and chronic inflammatory models. Our recent studies have shown that α-MSH covalently coupled to poly-L-glutamic acid (PGA-α-MSH) retains anti-inflammatory properties on rat monocytes. This study aimed to define the effects of PGA-α-MSH on dental pulp fibroblasts. Lipopolysaccharide (LPS)-stimulated fibroblasts incubated with PGA-α-MSH showed an early time-dependent inhibition of TNF-α, a late induction of IL-10, and no effect on IL-8 secretion. However, in the absence of LPS, PGA-α-MSH induced IL-8 secretion and proliferation of pulp fibroblasts, whereas free α-MSH inhibited this proliferation. Thus, PGA-α-MSH has potential effects in promoting human pulp fibroblast adhesion and cell proliferation. It can also reduce the inflammatory state of LPS-stimulated pulp fibroblasts observed in gram-negative bacterial infections. These effects suggest a novel use of PGA-α-MSH as an anti-inflammatory agent in the treatment of endodontic lesions. To better understand these results, we have also used the multilayered polyelectrolyte films as a reservoir for PGA-α-MSH by using not only PLL (poly-L-lysine) but also the Dendri Graft poly-L-lysines (DGL^{G4}) to be able to adsorb more PGA-α-MSH. Our results indicated clearly that, by using PGA-α-MSH, we increase not only the viability of cells but also the proliferation. We have also analyzed at the nanoscale by atomic force microscopy these nanostructured architectures and shown an increase of thickness and roughness in the presence of PGA-α-MSH incorporated into the multilayered film (PLL-PGA-α-MSH)$_{10}$ or (DGL^{G4}-PGA-α-MSH)$_{10}$ in accordance with the increase of the proliferation of the cells growing on the surface of these architectures. We report here the first use of nanostructured and functionalized multilayered films containing α-MSH as a new active biomaterial for endodontic regeneration.

KEYWORDS: pulp fibroblasts · inflammation · cytokines · melanocortin · multilayered films · nanostructured assemblies · Dendri Graft poly-L-lysines

ability to increase intracellular cAMP when activated.[2,9−12] α-MSH has been shown to inhibit the production and activity of proinflammatory mediators such as IL-1, TNF-α, IL-6, IL-13, and KC, the mouse homologue of human chemokine gro-α as well as the expression of adhesion molecules such as ICAM-1.[7,13] They also induce the production of the anti-inflammatory cytokine, IL-10.[14] These effects occur primarily by inhibiting IκBα degradation and NF-κB activation.[15−17]
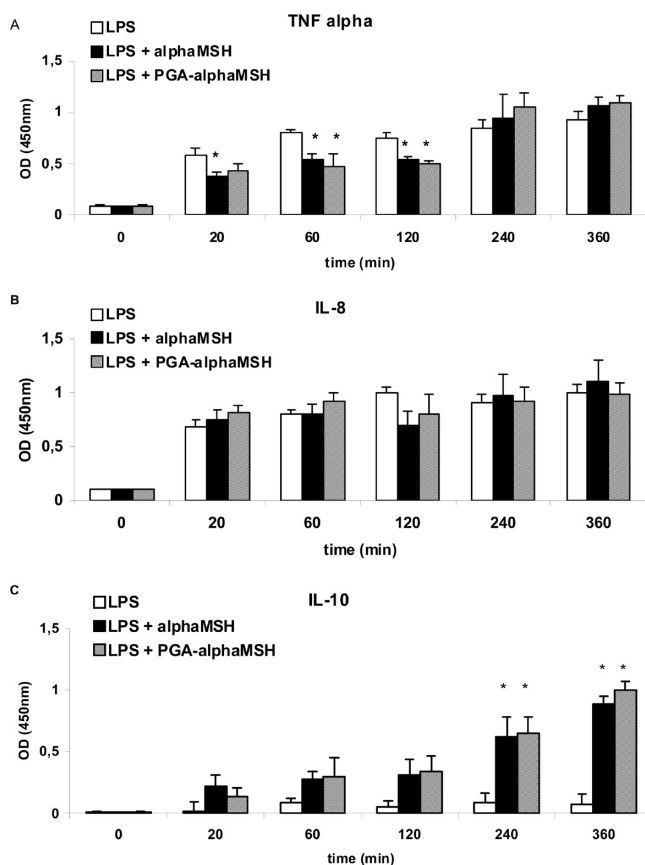
Figure 1. Kinetics of TNF-α (A), IL-8 (B), and IL-10 (C) production by LPS-stimulated pulp fibroblasts. Cells were incubated at a density of 5×10^5 cells/well in the presence of 10 ng mL^{-1} of LPS and 100 μg mL^{-1} of free α-MSH or of PGA-α-MSH for 20 min, 1 h, 2 h, 4 h, and 6 h: TNF-α production (A), IL-8 production (B), and IL-10 production (C). White bars represent the secretion with LPS alone; black bars represent the values obtained when cells were incubated with LPS + free α-MSH, and hatched bars represent the values obtained after incubation with LPS + PGA-α-MSH. An average of three measurements with the corresponding standard error is shown; *$P < 0.05$ vs LPS alone.

Most of these effects have been characterized in monocytes, keratinocytes, and dermal fibroblasts.

On dermal fibroblasts, differents studies reported clearly the anti-inflammatory effects of α-MSH and showed not only the inhibition of TNF-α signaling but also the suppression of the TGF-β1-induced expression of collagen.[18,19] This combined anti-inflammatory and anti-fibrogenic activity of α-MSH on this human fibroblastic cell type is of special value for the therapy of skin disorders where fibroblasts are aberrantly activated.[20−22]

However, the effects of α-MSH on pulp fibroblasts have not yet been described. The use of α-MSH could be an interesting way to explore control of the inflammatory activation of pulp fiblobasts after dental injury and therefore to keep teeth vitality.

The vitality of the pulp is fundamental to the functional life of the tooth and is a priority for targeting clinical management strategies. Dental pulp, as any other connective tissue, responds to aggression with the inflammation process, in order to eliminate pathogens

and allow repair. However, due to its particular features as the confinement in hard chamber and its unique blood irrigation and lymphatic circulation, a pulp inflammation process becomes hard to control and dissipate. Frequently, the pulp inflammation is so painful and clinically irreversible that the removal of the whole pulp is required.

Pulp fibroblasts are a key group of dental cells responsible for controlling a variety of matritial processes following dental injury. They play a central role in signaling various aspects of tissue regeneration. The control of the pulp fibroblast response is fundamental to control the pulp inflammation.[23−25]

Studies from our laboratory have shown that α-MSH can be covalently coupled to poly-L-lysine and incorporated into multilayer films, without changes in their biological properties,[26] and that such α-MSH derivatives retain anti-inflammatory properties *in vitro*.[27−29] In more recent studies, the α-MSH derivatives were coupled to the carrier polyion poly-L-glutamic acid (PGA), which leaves the anti-inflammatory C-terminal sequence Lys11-Pro12-Val13 of α-MSH peptides accessible. This PGA-α-MSH multilayer film was shown to have anti-inflammatory effects *in vivo* in a model of tracheal prosthesis.[29] The aim of this study was to investigate the effects of a biologically active film of PGA-α-MSH on human pulp fibroblasts including its effects on cytokine/chemokine expression.

RESULTS

Effects of α-MSH and PGA-α-MSH on Production of TNF-α, IL-10, and IL-8 by LPS-Stimulated Pulp Fibroblasts. Pulp fibroblasts were stimulated with LPS (10 ng mL^{-1}) in the presence of 100 μg mL^{-1} of either free α-MSH or PGA-α-MSH. The amount of TNF-α secreted by cells in the presence of LPS was significantly increased over a 6 h time period (Figure 1A). At early time points (20 min to 2 h), however, α-MSH and PGA-α-MSH significantly inhibited the amount of LPS-induced TNF-α secretion, while at later time points (4−6 h), this effect was lost. In contrast, no inhibition of LPS-induced IL-8 secretion was observed in the presence of 100 μg mL^{-1} of either α-MSH or PGA-α-MSH during this 6 h time period (Figure 1B). Furthermore, increasing the concentrations of both α-MSH and PGA-α-MSH 400 μg mL^{-1} did not change the amount of the IL-8 produced (data not shown). In contrast to these observations, both α-MSH and PGA-α-MSH induced significant levels of the anti-inflammatory cytokine, IL-10 (Figure 1C).

Effects of PGA-α-MSH on IL-8 Production by Pulp Fibroblasts in the Absence of LPS. Previous studies have shown that α-MSH stimulates the production of IL-8 by dermal fibroblasts.[30] To characterize the ability of PGA-α-MSH to stimulate IL-8, the levels of IL-8 expression were determined in LPS-free fibroblast cultures. Fibroblasts (pulp, Figure 2A, and NIH 3T3, Figure 2B) stimulated with PGA-α-MSH showed a time- and concentration-dependent
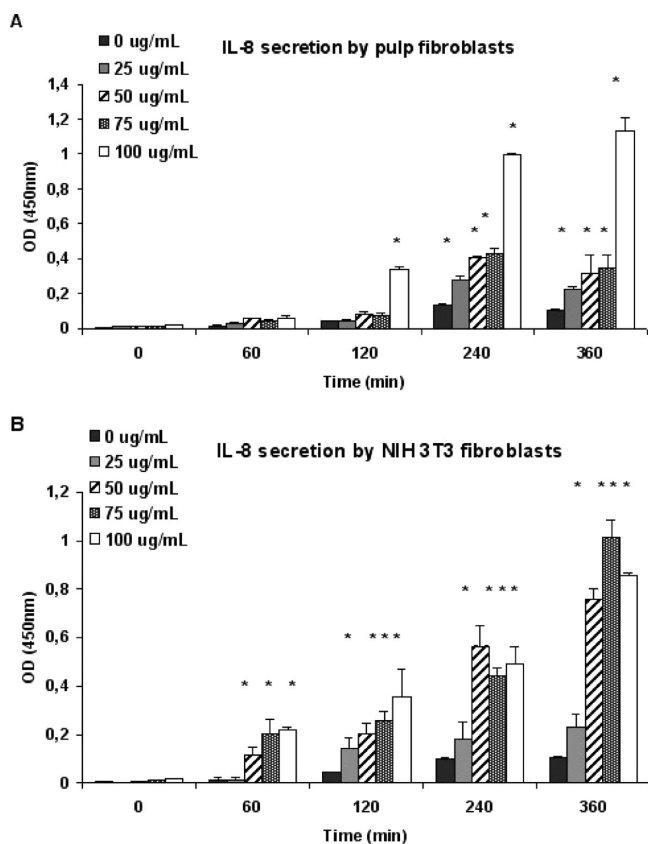
A

B

Figure 2. Kinetics of IL-8 production by pulp fibroblasts. Cells were incubated at a density of 5×10^5 cells/well in the absence of LPS. IL-8 production by human pulp (A) and NIH 3T3 (B) fibroblasts was measured after 0 min, 1 h, 2 h, 4 h, and 6 h of cell contact with different concentrations of PGA-α-MSH (0 μg mL^{-1}, black bars; 25 μg mL^{-1}, gray bars; 50 μg mL^{-1}, hatched bars; 75 μg mL^{-1}, dotted bars; 100 μg mL^{-1}, clear bars). An average of three measurements with the corresponding standard error is shown; *$P < 0.05$ vs control (PGA).

increase in IL-8 production, with NIH 3T3 fibroblasts being more sensitive than primary pulp fibroblasts. The first significant increase in IL-8 could be detected with 50 μg mL^{-1} of PGA-α-MSH on NIH 3T3 fibroblasts and with 100 μg mL^{-1} of PGA-α-MSH on pulp fibroblasts after 1 and 2 h contact, respectively.

PGA-α-MSH Internalization and Effects on cAMP Accumulation in Pulp Fibroblasts. Since α-MSH peptides are most effective when internalized by monocytes via their receptors,[9,10] the degree of internalization of PGA-α-MSH by pulp fibroblasts was assessed. Incubation of pulp fibroblasts with FITC-labeled PGA-α-MSH (100 μg mL^{-1}) resulted in a homogeneous fluorescence of the fibroblasts after 2 h, indicating internalization (Figure 3A). The effect of PGA-α-MSH on cAMP accumulation in pulp fibroblasts was then determined to ascertain whether it exerted its biological effects via activation of MCR receptors. Both the positive control, forskolin, and the nonselective agonist MTII significantly increased cAMP concentrations to 3367 $\pm$ 242 and 459 $\pm$ 14 fmol/well, respectively, above the basal level of 239 $\pm$ 36 fmol/well. In contrast, both the selective MC1R agonist (MS05)

and PGA-α-MSH failed to significantly increase cAMP accumulation at any of the concentrations tested (Figure 3B).

Effects of PGA-α-MSH on Pulp Fibroblast Proliferation and Adhesion. The ability of free α-MSH and PGA-α-MSH to promote proliferation and/or adhesion of fibroblasts was also determined. Cell viability was determined by trypan blue exclusion, and the proliferation was measured by the acidic phosphatase method (Figure 4).

We have also shown by confocal microscopy that the incubation of fresh seeded pulp fibroblasts with α-MSH (Figure 5A) PGA-α-MSH in solution (Figure 5B) indicates clearly that while α-MSH inhibits the proliferation of the cells (Figure 4B) (but not the viability, Figure 4A), the presence of α-MSH covalently coupled to PGA [PGA-α-MSH and (PLL-PGA)5-PLL-PGA-α-MSH] promotes adhesion. On the multilayered film, when PGA inhibits the adhesion of cells (Figure 6A), PGA-α-MSH on the multilayer film induces this adhesion (Figure 6B).

Pulp Fibroblast Behaviors Effects of PGA-α-MSH When Incorporated into the Multilayered Film (PLL-PGA-α-MSH)$_{10}$ by Using PLL or the Dendri Graft Poly-L-lysines (DGLs). In this study, we analyzed the effect of PGA-α-MSH on pulp fibroblast when PGA-α-MSH is not only adsorbed on the top of the multilayered films (see Figure 6) but also incorporated at each level as a reservoir for cells (PLL-PGA-α-MSH)$_{10}$ or by using the DGL^{G4},[31−33] to be able to adsorb more PGA-α-MSH and to increase the efficiency in terms of proliferation effect.

In Figure 7, we analyzed the proliferation and morphology of pulp fibroblasts growing on the surface of the multilayered films (PLL-PGA)$_{10}$ (A), (PLL-PGA-α-MSH)$_{10}$ (B), (DGL^{G4}-PGA)$_{10}$ (C), and (DGL^{G4}-PGA-α-MSH)$_{10}$ (D) followed by AlamarBlue. We have also analyzed by confocal microscopy morphology and actin organization these cells after 2 days of proliferation.

First we analyzed by quartz crystal microbalance (QCM) dissipation versus frequency shift of the multilayered films during their build-up process. Successive adsorptions on top of a SiO$_2$-coated quartz crystal sensor were monitored in situ by QCM for (PLL-PGA)$_{10}$ (A), (PLL-PGA-α-MSH)$_{10}$ (B), (DGL^{G4}-PGA)$_{10}$ (C), and (DGL^{G4}-PGA-α-MSH)$_{10}$ (D) multilayered films. In Figure 8, the values of frequency shift and dissipation are collected, and the linear regressions are added in the graph to follow the build.

In the next step, atomic force microscopy (AFM) was used to get additional information about the structure of these multilayered architectures at the nanoscale (Figure 9).
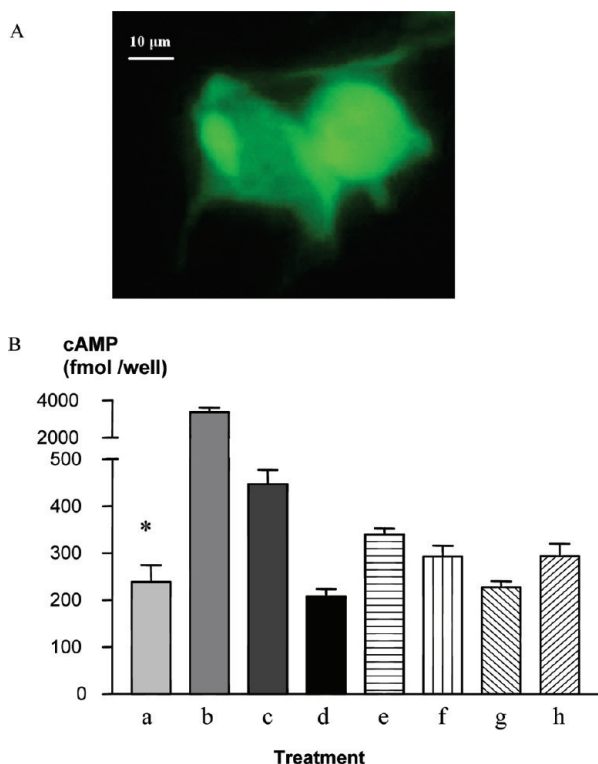
Figure 3. Internalization of FITC-labeled PGA-α-MSH and intracellular cAMP accumulation by pulp fibroblasts. (A) Fluorescent microscopy top view (green FITC channel) of pulp fibroblasts after 2 h of treatment with 100 μg mL^{-1} of PGA-α-MSH-FITC. (B) Intracellular cAMP accumulation. Pulp fibroblasts were incubated with (a) vehicle (negative control), (b) forskolin (3 μM), (c) MTII (10 μg mL^{-1}), (d) MS05 (10 μg mL^{-1}), PGA-α-MSH (e) 10 μg mL^{-1}, (f) 30 μg mL^{-1}, (g) 100 μg mL^{-1}, or (h) 300 μg mL^{-1} and cell-associated cAMP determined at the 30 min time point. Cell incubation with forskolin (used as a positive control) led to 3367 ± 242 fmol/well ($n = 6$). Data expressed as mean ± SEM of three experiments; $*P < 0.05$ vs vehicle (a).

Modification of dissipation can be correlated to increase the roughness of films analyzed by atomic force microscopy (AFM).[34] In this study, we have also analyzed the roughness and thickness of these nanostructured films (architectures A, B, C, and D) obtained by *in situ* AFM image height mode in buffer of these films (Figure 9 and Table 1).

DISCUSSION

Melanocortin peptides have been shown to possess anti-inflammatory effects in many experimental models of acute and chronic inflammation[35] and in human cells such as monocytes,[36] astrocytes, and keratinocytes. The biological effects of α-MSH are exerted partially *via* direct binding to their receptors (MCR) resulting in adenylate cyclase-mediated conversion of ATP to cyclic AMP[9,10] and inhibition of pro-inflammatory cytokines.[37−39] In addition to these anti-inflammatory properties in various cell types, α-MSH has also recently been shown to antagonize the effects of TGF-β on collagen synthesis by dermal fibroblasts.[19] These properties of α-MSH suggest that it might be useful for the

treatment of fibrotic disorders.[40] Due to these reported anti-inflammatory effects of α-MSH, we hypothesized that such agents might be therapeutically useful as anti-inflammatory agents for inflamed pulp, and thus, we have begun to investigate the effects of α-MSH and PGA-α-MSH on pulp fibroblasts.

To improve implant biocompatibility, polyelectrolyte multilayers on charged surfaces offer an important approach.[41−44] We have developed bioinert materials able to create, through surface modifications, a bioactive interface regulating biological responses.[27−29,45−49] We previously observed in a monocyte model, where we examined TNF-α and IL-10 secretions, that PGA-α-MSH induces a response similar to that of α-MSH in solution.[27] This was the basis for examining the effects of PGA-α-MSH on pulp fibroblasts.

As previously observed with monocytes, PGA-α-MSH, in contact with LPS-induced pulp fibroblasts, induces a bimodal anti-inflammatory response with an early inhibition of TNF-α production that is statistically significant after the first and second hour of activation and a later (4 h) statistically significant induction of the anti-inflammatory cytokine, IL-10.

These results have a significant impact on pulpal inflammation because TNF-α induces significant high levels of vascular growth factor mRNA gene expression in human pulp, which may promote apical expansion of the inflammation.[50] Therefore long-term expression of TNF-α may avoid the healing process as reactionary or reparative dentin formation, which acts to increase the barrier between the cells of the pulp and the injury.[51]

The induction of IL-10 by PGA-α-MSH is also crucial because IL-10 inhibits synthesis of most pro-inflammatory cytokines by dental pulp cells.[52]

Recently, it was reported that inflamed pulps present higher amounts of IL-1β and IL-8 than healthy pulps, and that pulp fibroblasts stimulated also by *Escherichia coli* LPS produce higher levels of IL-1β and IL-8 than the control group.[53] However, both α-MSH and PGA-α-MSH were unable to inhibit IL-8 release by LPS-stimulated pulp fibroblasts. The apparent discrepancy with studies in which α-MSH inhibited IL-1-induced IL-8 production in dermal fibroblasts[30] could be due to differing stimuli, LPS *versus* IL-1, or to the type of fibroblasts used. Even though NF-κB-mediated IL-8 gene expression can be induced by LPS through the CD14/TLR4 receptor complex or by IL-1 through the IL-1 receptor, the signaling pathways leading to IL-8 expression are partially different.[54,55] Furthermore, the involvement of α-MSH in these pathways is not identical.[13] In addition, since IL-1 is a better inducer of IL-8 than LPS in fibroblasts, the antagonist effects of α-MSH on IL-8 production might be more striking on IL-1-stimulated than on LPS-stimulated fibroblasts.

Free α-MSH is known to stimulate IL-8 expression by dermal fibroblasts.[30] To ascertain whether PGA-α-MSH retains this capacity, its effects on LPS-free pulp
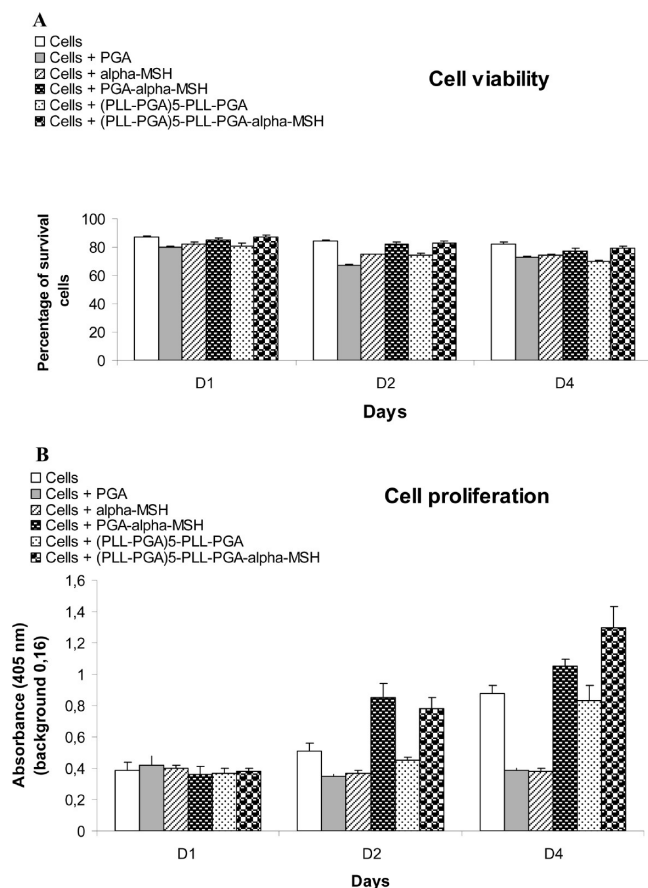
Figure 4. Viability and proliferation of pulp fibroblast. Viability of pulp fibroblast after 1 day (D1), 2 days (D2), or 4 days (D4). The percentage of viable cells has been calculated as follows: number of viable cells × 100/number of total cell with an average of eight measurements with the corresponding standard error (A). Cell proliferation has been checked by the acid phosphatase assay for quantifying the growth of adherent and nonadherent cells. The background corresponds to an absorbance of 0.16 at λ = 405 nm. An average of three measurements with the corresponding standard error was represented (B).

ered polyelectrolytes films by using different kinds of cells in terms of melanin production or cytokine production.[26,27] In this study, we checked first that PGA-α-MSH was still active when adsorbed on the top of the multilayered films (PGA-PLL). The objective here was to analyze the behaviors of the fibroblastic cells in terms of adhesion and proliferation in contact with the multilayered film in the presence or absence of PGA-α-MSH. To further characterize PGA-α-MSH potential, its effect on cell adhesion was determined in our model. PGA-α-MSH multilayer films contribute to adhesion and proliferation of human pulp fibroblasts, whereas unmodified PGA or free α-MSH clearly has no effect on cell adhesion and proliferation as compared to control fibroblast cultures. This could suggest that PGA-α-MSH and α-MSH somehow interact differently with the cells. This was confirmed by the diffuse fluorescence observed after contact between FITC-PGA-α-MSH and pulp fibroblasts and by the fact that cAMP levels were not significantly elevated after stimulation with PGA-α-MSH but were after treatment with MCR agonists, indicating that the effects of PGA-α-MSH are not specifically MCR receptor mediated. In fact, coupling α-MSH to PGA makes the C-terminal region of the peptide more accessible, enhancing the anti-inflammatory effects of the peptide without inducing cAMP accumulation, as has already been suggested for the peptide alone.[56]

To better understand the cells' behaviors when PGA-α-MSH is adsorbed on the top of the multilayered film (PGA-PLL)$_n$, we have analyzed the effects of PGA-α-MSH incorporated into the multilayered film (PLL-PGA-α-MSH)$_{10}$ as a reservoir for cells. We have also analyzed the effects when PLL was replaced by Dendri Graft poly-L-lysines (DGLs) in the same architecture (DGL^{G4}-PGA-α-MSH)$_{10}$.

and NIH 3T3 fibroblasts were evaluated. Similar IL-8 secretion profiles were found, confirming that the stimulation more than the cell type is important for free-α-MSH or PGA-α-MSH overall effect. Recently, we and others reported clearly that the PGA-α-MSH kept its full activities when adsorbed on the top of the multilay-
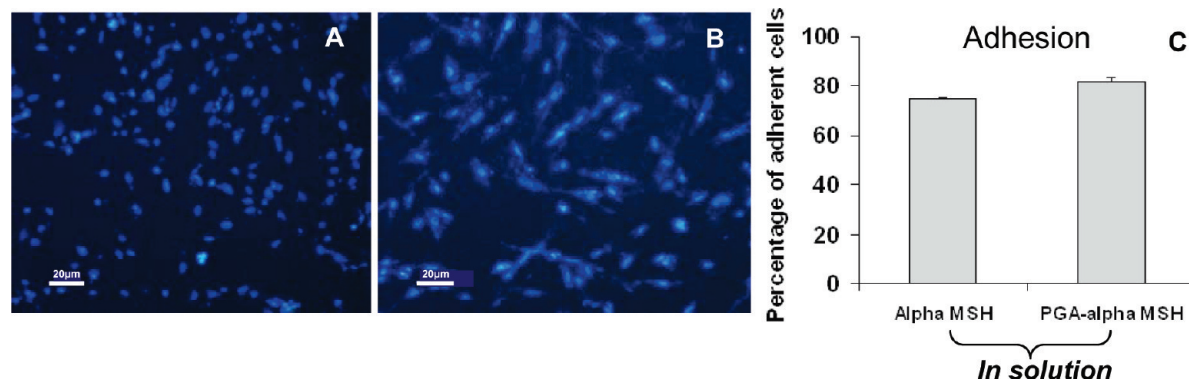

Figure 5. Pulp fibroblast morphological changes after 2 days of culture. Cell morphology of pulp fibroblasts after 2 days of culture seeded in the presence of α-MSH (A) or PGA-α-MSH (B). After 2 days, the quantification of the adherent cells in the presence of α-MSH or PGA-α-MSH in solution was analyzed (C).
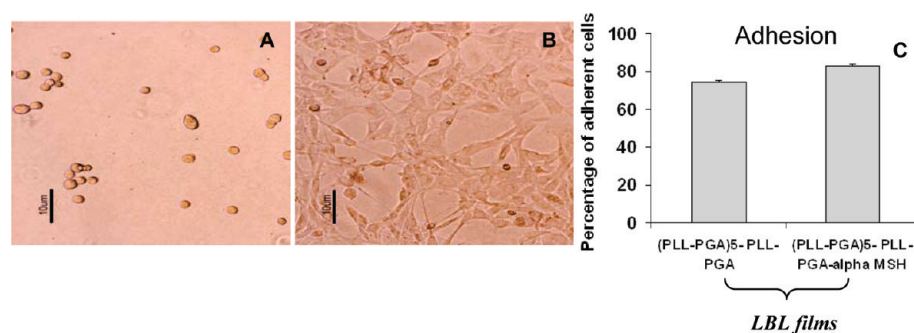
Figure 6. Pulp fibroblast morphological changes after 2 days of culture. Cell morphology and quantification of adherent cells of pulp fibroblasts after 2 days of culture seeded on the multilayered films (PLL-PGA)$_5$-PLL-PGA (A) or (PLL-PGA)5-PLL-PGA-α-MSH (B). Quantification of adherent cells on the LBL films (C).

In Figure 7, we analyzed proliferation and morphology of pulp fibroblasts growing on the surface of the multilayered films (PLL-PGA)$_{10}$ (A), (PLL-PGA-α-MSH)$_{10}$ (B), (DGL^{G4}-PGA)$_{10}$ (C), and (DGL^{G4}-PGA-α-MSH)$_{10}$ (D) followed by AlamarBlue and confocal microscopy (morphology). Our results indicated clearly an increase of cell proliferation in the presence of PGA-α-MSH when adsorbed on PLL or DGL^{G4} as a reservoir for cells. These results are in accordance with the results obtained by adsorption of only one layer of PGA-α-MSH on the top of the multilayered film (PLL-PGA)$_5$-PLL. To better understand these results, we analyzed at the nanoscale these multilayered films (architectures A, B, C, and D).

First, we analyzed by QCM dissipation *versus* frequency shift of the multilayered films during their build-up process. Successive adsorptions on top of a SiO$_2$-coated quartz crystal sensor were monitored *in situ* by QCM for (PLL-PGA)$_{10}$ (A), (PLL-PGA-α-MSH)$_{10}$ (B), (DGL^{G4}-PGA)$_{10}$ (C), and (DGL^{G4}-PGA-α-MSH)$_{10}$ (D) multilayered films. In Figure 8, the values of frequency shift and dissipation are collected, and the linear regressions are added in the graph to follow the build.

From Figure 8, when the evolution of dissipation is plotted *versus* evolution of frequency, it is evident that using DGL^{G4} and/or PGA-α-MSH during the build-up of the film have significantly modified the viscoelasticity

value. The ratio R goes from 1.0×10^{-3} for (PLL-PGA)$_{10}$ (A) film to 10.0×10^{-3} for (PLL-PGA-α-MSH)$_{10}$ (B) or (DGL^{G4}-PGA)$_{10}$ (C) films. Interestingly, by using both DGL^{G4} and PGA-α-MSH in the case of (DGL^{G4}-PGA-α-MSH)$_{10}$ (D), the ratio R increases until 14.0×10^{-3} (Table 1).

The evolution of $\Delta f/\nu$ showed a regular film deposition starting with the first layer of PLL. The increase in $-\Delta f/\nu$ with the number of deposited layers suggested that regular film deposition occurred.

In the next step, atomic force microscopy (AFM) was used to get additional information about the structure of these multilayered architectures (Figure 9).

Modification of dissipation can be correlated to increase the roughness of films analyzed by AFM.[34] In this study, we have also analyzed the roughness and thickness of these nanostructured films (architectures A, B, C, and D) obtained by *in situ* AFM image height modes in buffer of these films (Figure 9 and Table 1). In Figure 9, the films made of alternating layers of PLL or DGL^{G4} and PGA or PGA-α-MSH were examined *in situ* by AFM in the liquid phase. The film thickness was evaluated by scratching the film with the AFM tip and was estimated to be 7.7 nm for (PLL-PGA)$_{10}$ without -α-MSH, 307 nm for (PLL-PGA-α-MSH)$_{10}$, and 532 nm for (DGL^{G4}-PGA-α-MSH)$_{10}$ in the presence of both DGL^{G4}
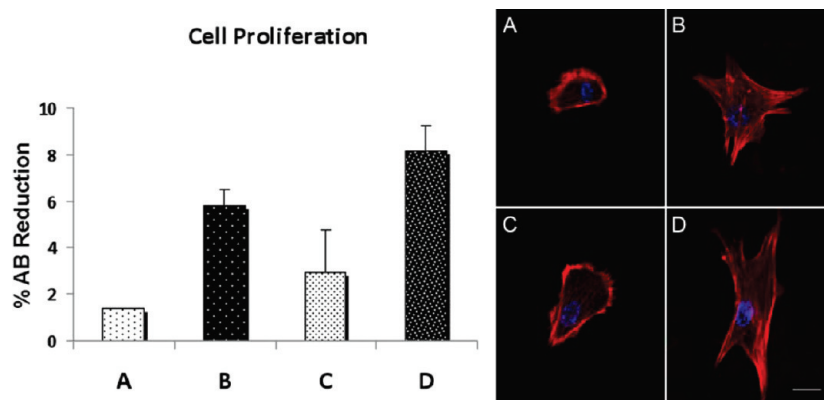

Figure 7. Proliferation and morphology of pulp fibroblasts growing on the surface of the multilayered films. Proliferation of pulp fibroblast after 2 days of culture on the surface of the multilayered films (PLL-PGA)$_{10}$ (A), (PLL-PGA-αMSH)$_{10}$ (B), (DGL^{G4}-PGA)$_{10}$ (C), and (DGL^{G4}-PGA-αMSH)$_{10}$ (D) followed by AlamarBlue (left panel). Morphology and actin organization of cells (fixation after 2 days of proliferation) observed by confocal microscopy (right panel): Alexa Fluor 546-labeled phalloidin (red) and DAPI (blue), scale bar = 20 μm.
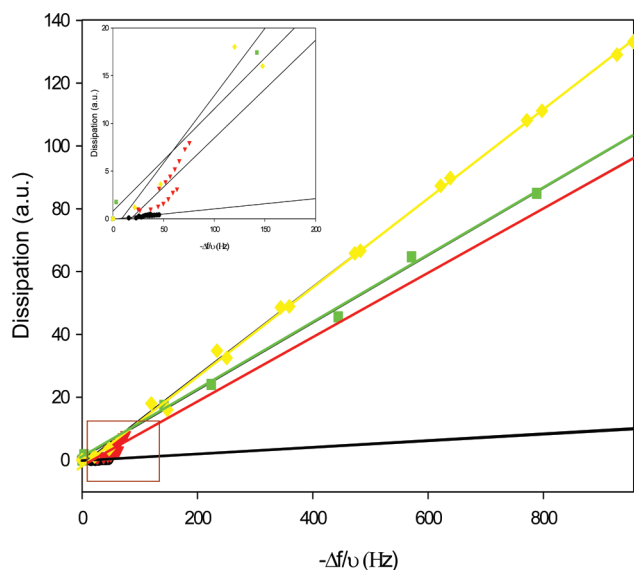
Figure 8. Dissipation *versus* frequency shift analysis by QCM of the multilayered films during their build-up process. Successive adsorptions on top of a SiO₂-coated quartz crystal sensor were monitored *in situ* by QCM for (PLL-PGA)₁₀ (●), (PLL-PGA-α-MSH)₁₀ (▼), (DGL^G4-PGA)₁₀ (■), and (DGL^G4-PGA-α-MSH)₁₀ (◆) multilayered films. Values of frequency shift and dissipation are collected, and the linear regressions are added in the graph to follow the build-up of each film. The zoom of the low values of dissipation and frequency is presented in the inset.

and PGA-α-MSH deposited materials compared to the deposited DGL^G4 in the architecture (DGL^G4-PGA)₁₀ without α-MSH estimated to only 8.2 nm. The roughness was also analyzed (Table 1) and was still in line with the

results obtained concerning the proliferation and the morphology of cells growing on the surface of these nanostructured films with an increase of the roughness (rms) from 4.1 nm without α-MSH to 66.1 nm with α-MSH. Interestingly, by using DGL^G4, the roughness (rms) goes from 2.3 nm without α-MSH to 18.7 nm with α-MSH. In this case, when we combine both DGL^G4 and α-MSH, we do not have more roughness but more thickness. These results could be explained by an intralayer process increasing the film cohesion and increasing the film hydration.

CONCLUSION

Millions of teeth are saved each year by root canal therapy. Although current treatment modalities offer high levels of success for many conditions, an ideal form of therapy might consist of regenerative approaches in which diseased or necrotic pulp tissues are removed and replaced with healthy pulp tissue to revitalize teeth.[57]

Pulp fibroblast plays a central role in signaling various aspects of tissue regeneration. The control of the pulp fibroblast response is fundamental to control the pulp inflammation. We have shown that free PGA-α-MSH can modulate the activation of human pulp fibroblasts and can regulate the inflammatory fi-
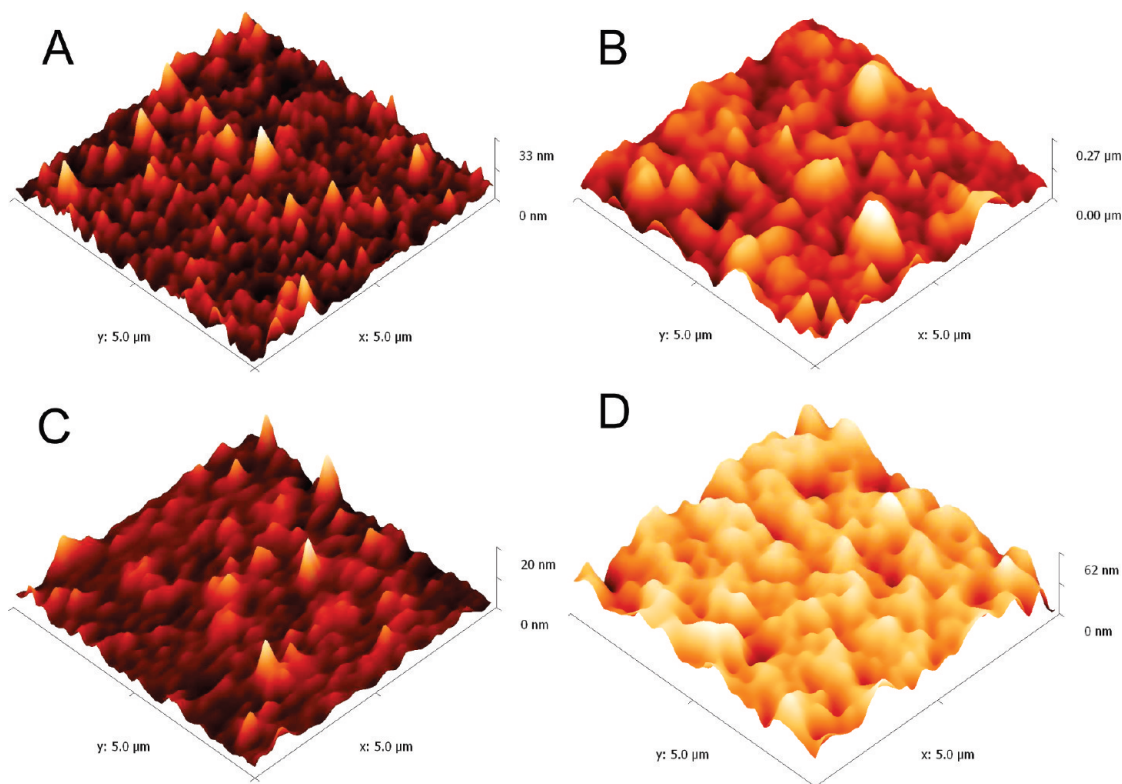

Figure 9. Height mode AFM images in buffer of the multilayered films. *In situ* AFM images (5 × 5 μm²) of the multilayered films (PLL-PGA)₁₀ (A), (PLL-PGA-α-MSH)₁₀ (B), (DGL^G4-PGA)₁₀ (C), and (DGL^G4-PGA-α-MSH)₁₀ (D).

TABLE 1. Physical Characterization of the Multilayered Films[a]

nanostructured films	roughness rms (nm)	thickness (nm)	$\Delta D/(\Delta f/\nu)$ (QCM)
A	4.1 ± 0.3	7.7 ± 2.2	0.01 ± 0.0015
B	66.1 ± 13.6	307 ± 48	0.10 ± 0.026
C	2.3 ± 0.7	8.2 ± 1.1	0.10 ± 0.018
D	18.7 ± 2.3	538 ± 100	0.14 ± 0.001

[a]Roughness, thickness, and $\Delta D/(\Delta f/\nu)$ analysis of the multilayered films (PLL-PGA)$_{10}$ (A), (PLL-PGA-α-MSH)$_{10}$ (B), (DGL^{G4}-PGA)$_{10}$ (C), and (DGL^{G4}-PGA-α-MSH)$_{10}$ (D) obtained by AFM and QCM .

broblast's environment as well as the ability of the fibroblast to adhere.

We have also investigated whether PGA-α-MSH could induce adhesion when in contact with a multilayered film finding an increase in adhesion and prolifera-

tion, while PGA alone or free α-MSH inhibited this mechanism. In conclusion, this study highlights that PGA-α-MSH can not only modulate pro- and anti-inflammatory cytokines but also promote adhesion of pulpal fibroblasts. Therefore, these effects of PGA-α-MSH may have important regulatory functions in extracellular matrix composition.

Although the mechanism by which PGA-α-MSH can stimulate all of these responses in human pulp fibroblasts has not yet been elucidated, PGA-α-MSH may, nevertheless, have important regulatory functions to modulate pulpal inflammation, which causes pulpitis followed by apical periodontitis. We report here the first use of nanostructured and functionalized multilayered films containing α-MSH as a new active biomaterial for endodontic regeneration.

MATERIALS AND METHODS

Chemicals. The α-MSH analogue, HS-CH$_2$CH$_2$-Ser-Tyr-Ser-Nle-Glu-His-D-Phe-Arg-Trp-Gly-Lys-Pro-Val-COOH, was obtained from Neosystem (Strasbourg, France). Poly-L-glutamic acid (PGA), poly-L-lysine hydrobromide (PLL), N-hydroxysulfosuccinimide, lipopolysaccharide (LPS) from E. coli 026:B6, and phorbol ester 12-O tetradecanoyl phorbol 13 acetate (TPA) were obtained from Sigma (St. Quentin, France).

Synthesis of PGA-α-MSH Films. The α-MSH peptide was covalently coupled to poly-L-glutamic acid (PGA) and used free or incorporated into the polyelectrolyte multilayer films (PLL-PGA)$_n$-PLL as previously described.[27,29]

Synthesis of Dendri Graft Poly-L-lysines (DGLs). DGLs were prepared as described in a recent publication.[31] In brief, N$^\epsilon$-TFA-L-lysine-NCA prepared according to a method reported in the literature[32] was dissolved in an aqueous H$_2$—CO$_3$/HCO$_3$Na solution (pH 6.5),[33] leading, after 30 min, to oligo-N$^\epsilon$-TFA-L-lysine, which precipitates and is isolated by filtration. The protecting group is removed with 150 mL of water—methanol ammonia solution at pH 11 (15 h at 40 °C). Following partial solvent removal at reduced pressure, the remaining solution was freeze-dried, affording to a first-generation oligo(L-lysine) of DPn = 8 and low polydispersity (1.2). By repeating the same polymerization procedure in the presence of the first-generation oligo(L-lysine), second-generation DGL (DGL^{G2}) was obtained (DPn = 48 and polydispersity = 1.3) following deprotection and freeze-drying. The third-generation DGL (DGL^{G3}) was obtained (DPn = 123 and polydispersity = 1.4) under the same conditions using DGL^{G2}. The fourth-generation DGL (DGL^{G4}) was obtained (DPn = 365 and polydispersity = 1.3) under the same conditions using DGL^{G3}. The structures of DGL^{G2}, DGL^{G3}, and DGL^{G4} were established by ^{1}H and ^{13}C NMR. In this study, we have used the fourth-generation DGL^{G4}.

Polyelectrolyte Multilayered Film Preparation. For all biological activity experiments, polyelectrolyte multilayer films were prepared on glass coverslips (CML, France) and pretreated with 10^{-2} M SDS and 0.12 N HCl for 15 min at 100 °C, and then extensively rinsed with deionized water. The glass coverslips were then deposited in 24-well plates (Nunc, Denmark). A precursor film constituted by PLL-(PGA-PLL) was built by alternating immersion of the plates during 20 min in the respective polyelectrolyte solutions (300 μL) at the respective concentrations of 1 mg/mL for PGA and PLL in the presence of 0.15 M NaCl at pH = 7.4. PGA-α-MSH is negatively charged and was always adsorbed on a film terminating with a layer of positively charged PLL. After each deposition step, the coverslips were rinsed three times during 5 min with deionized water. All of the films were sterilized for 10 min by exposure to ultraviolet (UV) light (254 nm, 30 W, illumination distance 20 cm). Before use, all films were equili-

brated in contact with 1 mL of RPMI medium (see Cell Culture) without serum.

Cell Culture. Human pulp fibroblasts were obtained from human third molar germ tissue extracted for orthodontic reasons (Dental School, Strasbourg). These tissues were used with the patient's informed consent and approval by the Research Ethics Committee. Human pulp fibroblasts and mouse embryo fibroblasts (NIH 3T3, a gift of IGBMC, Strasbourg, France) were cultured in Dulbecco's modified Eagle's medium (D-MEM) containing 1% antimicotic solution and 10% FBS (Life Technologies, Paisley, UK). The cultures were incubated at 37 °C in a humidified atmosphere of 5% CO$_2$. When the cells reached subconfluence, they were harvested with trypsin and subcultured. The fibroblast cultures used for all experiments were from passages three to six.

Cell Viability and Proliferation. Cell viability was determined by trypan blue exclusion. Cell proliferation was measured by the acid phosphatase method. Briefly, cells were washed with 300 mL of PBS. The buffer added to each well contains 0.1 M sodium acetate (pH 5.5), 0.1% of Triton X-100, and 10 mM of p-nitrophenyl phosphate [pNPP] (Sigma, St. Quentin, France). After a 3 h incubation at 37 °C with 5% CO$_2$, the reaction was stopped by the addition of 1 N sodium hydroxide, and the absorbance was measured by a spectrophotometer at 405 nm (Labsystems, iEMS Reader MF, Gibco). Cell viability and proliferation were measured at 24 and 96 h. Cell spreading and adhesion were observed by confocal microscopy.

AlamarBlue (Serotec) was used to assess cellular proliferation. The AlamarBlue test is a nontoxic, water-soluble, colorimetric redox indicator that changes color in response to cell metabolism. In this study, 5×10^4 pulp fibroblasts were seeded on the top of LbL-coated 14 mm diameter coverslips ($n = 3$) placed on 24-well plates. After 2 days of culture, cells were incubated in 10% AlamarBlue/D-MEM solution in a humidified atmosphere at 37 °C and 5% CO$_2$. After 6 h, 100 mL of incubation media was transferred to 96-well plates and measured at 590 and 630 nm in order to determine the percentage of AlamarBlue reduction.

Immunofluorescence. After 2 days of proliferation, cells were fixed with 4% PFA during 1 h, permeabilized with 0.1% Triton X-100 for 1 h, and incubated for 20 min with Alexa Fluor 546-conjugated phalloidin (Molecular Probes) for F-actin labeling and 5 min with 200 nM DAPI (Sigma) for nuclear staining. Cells were mounted on microscope slides using Vectashield (Vector) and imaged by confocal microscopy (Zeiss, LSM 510).

Cell Activation. Fibroblasts (5×10^5) were seeded in 24-well plates (Nunc, CML, Nemours, France) and incubated with LPS (10 ng mL^{-1}) from E. coli in the presence or absence of free α-MSH or PGA-α-MSH coupled peptides, in D-MEM without FBS. At different time points of incubation, cells were centrifuged and the levels of TNF-α, IL-10, or IL-8 in cell-free superna-

tants were determined using commercially available ELISA kits (Endogen, Woburn, MA). Studies of the effects of multilayer films consisting of PGA-α-MSH coupled peptides were conducted by seeding 5×10^5 cells directly onto the film in a 24-well plate as previously described.[26] All experiments were performed at least three times.

Intracellular cAMP. Pulp fibroblasts (1×10^5) were plated in 24-well plates in D-MEM containing 1% antimicotic solution and 10% FBS (Life Technologies, Paisley, UK). The cultures were incubated at 37 °C in a humidified atmosphere of 5% CO_2 and allowed to adhere for 2 h. Cells were then washed and incubated with 3 μM forskolin (positive control), the MC3/4R agonist MTII (10 μg mL^{-1}), the MC1R agonist MS05 (10 μg mL^{-1}), and PGA-α-MSH (10−300 μg mL^{-1}) in the presence of 1 mM isobutylmethylxanthine in serum-free medium and incubated for 30 min at 37 °C in a humidified atmosphere of 5% CO_2. A nontreated group incubated in serum-free medium alone served as a negative control. Cell supernatants were then removed, and the cells were lysed. Intracellular cAMP was quantified using a commercially available enzyme immunoassay kit and a standard curve constructed with 0−3200 fmol μg mL^{-1} cAMP (Amersham Bioscience, Little Chalfont, UK).

Quartz Crystal Microbalance. The films were monitored *in situ* with a quartz crystal microbalance using an axial flow chamber QAFC 302 (QCM-D, D300, Q-Sense, Götenborg, Sweden). QCM works by measuring the resonance frequency shift (Δf) of a quartz crystal induced by polyelectrolyte or protein adsorption onto the crystal in comparison to the crystal in contact with buffer. Changes in the resonance frequencies were measured at the third overtone ($\nu = 3$), corresponding to the 15 MHz resonance frequency. A shift in $\Delta f/\nu$ can be related in a first approximation to a variation of the mass adsorbed to the crystal by the Sauerbrey relation: $m = -C\Delta f/\nu$, where C is a constant characteristic of the crystal used (in our case, $C = 17.7$ ng cm^{-2} Hz^{-1}). The qualitative information about the viscoelastic properties of the film can be analyzed by using the ratio R: $\Delta D/(f/\nu)$. An increasing value of this ratio indicates a decreasing of stiffness of the deposited material.

Atomic Force Microscopy. The images were obtained in contact mode in liquid conditions with the Solver Pro from NT-MDT (Moscow, Russia). Cantilevers with a spring constant of 0.03 N/m and with silicon nitride tips were used (Model MSCT-AUHW Park Scientific, Sunnyvale, CA). Several scans were performed over a given surface area. These scans had to give reproducible images to ascertain that there is no sample damage induced by the tip. Deflection and height mode images are scanned simultaneously at a fixed scan rate (between 2 Hz) with a resolution of 512×512 pixels. For all observations, the samples were kept under liquid (build-up buffer).

Confocal Laser Scanning Microscopy (CLSM). CLSM observations were documented with a Zeiss LSM 510 microscope using a ×40/1.4 oil immersion objective at 0.4 μm z-section intervals. FITC fluorescence was detected after excitation at 488 nm with a 488 nm cutoff dichroic mirror and a 505−530 nm emission band-pass filter (green). All experiments were performed with cells in solution.

Statistical Analysis. All values are expressed as mean ± SEM, and all experiments were repeated at least three times. Statistical analysis was performed using the Mann−Whitney U test. A probability p value <0.05 was considered significant to reject the null hypothesis.

REFERENCES AND NOTES

1. Bashutski, J. D.; Wang, H. L. Periodontal and Endodontic Regeneration. *J. Endod.* **2009**, *35*, 321–328.
2. Böhm, M.; Luger, T. A.; Tobin, D. J.; García-Borrón, J. C. Melanocortin Receptor Ligands: New Horizons for Skin Biology and Clinical Dermatology. *J. Invest. Dermatol.* **2006**, *126*, 1966–1975.
3. Boston, B. A. The Role of Melanocortins in Adipocyte Function. *Ann. N.Y. Acad. Sci.* **1999**, *885*, 75–84.
4. Dumont, L. M.; Wu, C. S.; Tatnell, M. A.; Cornish, J.; Mountjoy, K. G. Evidence for Direct Actions of Melanocortin Peptides on Bone Metabolism. *Peptides* **2005**, *26*, 1929–1935.
5. Catania, A.; Airaghi, L.; Colombo, G.; Lipton, J. M. α-Melanocyte-Stimulating Hormone in Normal Human Physiology and Disease States. *Trends Endocrinol. Metab.* **2000**, *11*, 304–308.
6. Catania, A.; Gatti, S.; Colombo, G.; Lipton, J. M. Targeting Melanocortin Receptors as a Novel Strategy To Control Inflammation. *Pharmacol. Rev.* **2004**, *56*, 1–29.
7. Lam, C. W.; Getting, S. J. Melanocortin Receptor Type 3 as a Potential Target for Anti-inflammatory Therapy. *Curr. Drug Targets* **2004**, *3*, 311–315.
8. Kokot, A.; Sindrilaru, A.; Schiller, M; Sunderkötter, C.; Kerkhoff, C.; Eckes, B.; Scharffetter-Kochanek, K.; Luger, T. A.; Bohm, M. α-Melanocyte-Stimulating Hormone Suppresses Bleomycin-Induced Collagen Synthesis and Reduces Tissue Fibrosis in a Mouse Model of Scleroderma: Melanocortin Peptides as a Novel Treatment Strategy for Scleroderma. *Arthritis Rheum.* **2009**, *60*, 592–603.
9. Wikberg, J. E.; Muceniece, R.; Mandrika, I.; Prusis, P.; Lindblom, J.; Post, C.; Skottner, A. New Aspects on the Melanocortins and Their Receptors. *Pharmacol. Res.* **2000**, *42*, 393–420.
10. Gantz, I.; Fong, T. M. The Melanocortin System. *Am. J. Physiol. Endocrinol. Metab.* **2003**, *284*, 468–474.
11. Wong, W.; Minchin, R. F. Binding and Internalization of the Melanocyte Stimulating Hormone Receptor Ligand [Nle4, D-Phe7] α-MSH in B16 Melanoma Cells. *Int. J. Biochem. Cell Biol.* **1996**, *28*, 1223–1232.
12. Getting, S. J. Targeting Melanocortin Receptors as Potential Novel Therapeutics. *Pharmacol. Ther.* **2006**, *111*, 1–15.
13. Sarkar, A.; Sreenivasan, Y.; Manna, S. K. α-Melanocyte-Stimulating Hormone Inhibits Lipopolysaccharide-Induced Biological Responses by Downregulating CD14 from Macrophages. *FEBS Lett.* **2003**, *553*, 286–294.
14. Luger, T. A.; Scholzen, T. E.; Brzoska, T.; Bohm, M. New Insights into the Functions of α-MSH and Related Peptides in the Immune System. *Ann. N.Y. Acad. Sci.* **2003**, *994*, 133–140.
15. Ichiyama, T.; Campbell, I. L.; Furukawa, S.; Catania, A.; Lipton, J. M. Autocrine α-Melanocyte-Stimulating Hormone Inhibits NF-κB Activation in Human Glioma. *J. Neurosci. Res.* **1999**, *58*, 684–689.
16. Ichiyama, T.; Sakai, T.; Catania, A.; Barsh, G. S.; Furukawa, S.; Lipton, J. M. Inhibition of Peripheral NF-κB Activation by Central Action of α-Melanocyte-Stimulating Hormone. *J. Neuroimmunol.* **1999**, *99*, 211–217.
17. Manna, S. K.; Aggarwal, B. B. α-Melanocyte Stimulating Hormone Inhibits the Nuclear Transcription Factor NF-κB Activation by Various Inflammatory Agents. *J. Immunol.* **1998**, *161*, 2873–2880.
18. Hill, R.; MacNeil, S.; Haycock, J. W. Melanocyte Stimulating Hormone Peptides Inhibit TNF-α Signaling in Human Dermal Fibroblast Cells. *Peptides* **2006**, *27*, 421–430.
19. Bohm, M.; Raghunath, M.; Sunderkotter, C.; Schiller, M.; Stander, S.; Brzoska, T.; Cauvet, T.; Schioth, H. B.; Schwarz, T.; Luger, T. A. Collagen Metabolism is a Novel Target of the Neuropeptide α-Alpha-Melanocyte-Stimulating Hormone. *J. Biol. Chem.* **2004**, *279*, 6959–6966.
20. Hill, R. P.; Wheeler, P.; MacNeil, S.; Haycock, J. W. α-Melanocyte Stimulating Hormone Cytoprotective Biology in Human Dermal Fibroblast Cells. *Peptides* **2005**, *26*, 1150–1158.

21. Hedley, S. J.; Layton, C.; Heaton, M.; Chakrabarty, K. H.; Dawson, R. A.; Gawkrodger, D. J.; MacNeil, S. Fibroblasts Play a Regulatory Role in the Control of Pigmentation in Reconstructed Human Skin from Skin Types I and II. *Pigm. Cell Res.* **2002**, *15*, 49–56.

22. Schiller, M.; Dennler, S.; Anderegg, U.; Kokot, A.; Simon, J. C.; Luger, T. A.; Mauviel, A.; Bohm, M. Increased cAMP Levels Modulate Transforming Growth Factor (TGF-β)/SMAD-Induced Expression of Extracellular Matrix Components and Other Key Fibroblast Effector Functions. *J. Biol. Chem.* **2009**, *26*, 1–22.

23. Witherspoon, D. E. Vital Pulp Therapy with New Materials: New Directions and Treatment Perspectives—Permanent Teeth. *Pediatr. Dent.* **2008**, *30*, 220–224.

24. Goldberg, M.; Farges, J. C.; Lacerda-Pinheiro, S.; Six, N.; Jegat, N.; Decup, F.; Septier, D.; Carrouel, F.; Durand, S.; Chaussain-Miller, C. A.; *et al.* Inflammatory and Immunological Aspects of Dental Pulp Repair. *Pharmacol. Res.* **2008**, *58*, 137–147.

25. Wisithphrom, K.; Windsor, L. J. The Effects of Tumor Necrosis Factor-α, Interleukin-1β, Interleukin-6, and Transforming Growth Factor-β1 on Pulp Fibroblast Mediated Collagen Degradation. *J. Endod.* **2006**, *32*, 853–861.

26. Chluba, J.; Voegel, J. C.; Decher, G.; Erbacher, P.; Schaaf, P.; Ogier, J. Peptide Hormone Covalently Bound to Polyelectrolytes and Embedded into Multilayer Architectures Conserving Full Biological Activity. *Biomacromolecules* **2001**, *2*, 800–805.

27. Jessel, N.; Lavalle, Ph.; Meyer, F.; Audouin, F.; Frisch, B.; Schaaf, P.; Ogier, J.; Decher, G.; Voegel, J. C. Control of Monocyte Morphology on and Response to Model Surfaces for Implants Equipped with Anti-inflammatory Agents. *Adv. Mater.* **2004**, *16*, 1507–1511.

28. Jessel, N.; Falvey, P.; Darcy, R.; Haikel, Y.; Schaaf, P.; Voegel, J. C. Build-up of Polypeptide Multilayer Coatings with Anti-inflammatory Properties Based on the Embedding of Piroxicam−Cyclodextrin Complexes. *Adv. Funct. Mater.* **2004**, *14*, 174–182.

29. Schultz, P.; Vautier, D.; Richert, L.; Jessel, N.; Haikel, Y.; Schaaf, P.; Voegel, J. C.; Ogier, J.; Debry, C. Polyelectrolyte Multilayer Functionalized by a Synthetic Analogue of an Anti-inflammatory Peptide, α-MSH, for Coating a Tracheal Prosthesis. *Biomaterials* **2005**, *26*, 2621–2630.

30. Bohm, M.; Schulte, U.; Kalden, U.; Luger, T. A. α-Melanocyte-Stimulating Hormone Modulates Activation of NF-kappa κB and AP-1 and Secretion of Interleukin-8 in Human Dermal Fibroblasts. *Ann. N.Y. Acad. Sci.* **1999**, *885*, 277–286.

31. Collet, H.; Souaid, E.; Cottet, H.; Deratani, A.; Boiteau, L.; Dessalces, G.; Rossi, J. C.; Commeyras, A.; Pascal, R. An Expeditious Multigram-Scale Synthesis of Lysine Dendrigraft (DGL) Polymers by Aqueous *N*-Carboxyanhydride Polycondensation. *Chem.—Eur. J.* **2010**, *16*, 2309–2316.

32. Collet, H.; Bied, C.; Mion, L.; Taillades, J.; Commeyras, A. A New Simple and Quantitative Synthesis of α-Aminoacid-*N*-Carboxyanhydrides (Oxazolidines-2,5-dione). *Tetrahedron Lett.* **1996**, *37*, 9043–9046.

33. Commeyras, A.; Collet, H.; Boiteau, L.; Taillades, J.; Vandenabeele-Trambouze, O.; Cottet, H.; Biron, J. P.; Plasson, R.; Mion, L.; Lagrille, O.; *et al.* Prebiotic Synthesis of Sequential Peptides on the Hadean Beach by a Molecular Engine Working with Nitrogen Oxides as Energy Sources. *Polym. Int.* **2002**, *51*, 661–665.

34. Jessel, N.; Oulad-Abdeighani, M.; Meyer, F.; Lavalle, P.; Haikel, Y.; Schaaf, P. Voegel, J.C. Multiple and Time-Scheduled in Situ DNA Delivery Mediated by beta-Cyclodextrin Embedded in a Polyelectrolyte Multilayer. *Proc. Natl. Acad. Sci. U.S.A.* **2006**, *103*, 8618–8621.

35. Mason, M. J.; Van Epps, D. Modulation of IL-1, Tumor Necrosis Factor, and C5a-Mediated Murine Neutrophil Migration by α-Melanocyte-Stimulating Hormone. *J. Immunol.* **1989**, *142*, 1646–1651.

36. Colombo, G.; Buffa, R.; Bardella, M. T.; Garofalo, L.; Carlin, A.; Lipton, J. M.; Catania, A. Anti-inflammatory Effects of α-Melanocyte-Stimulating Hormone in Celiac Intestinal Mucosa. *Neuroimmunomodulation* **2002**, *10*, 208–216.

37. Delgado, R.; Carlin, A.; Airaghi, L.; Demitri, M. T.; Meda, L.; Galimberti, D.; Baron, P.; Lipton, J. M.; Catania, A. Melanocortin Peptides Inhibit Production of Proinflammatory Cytokines and Nitric Oxide by Activated Microglia. *J. Leukocyte Biol.* **1998**, *63*, 740–745.

38. Taherzadeh, S.; Sharma, S.; Chhajlani, V.; Gantz, I.; Rajora, N.; Demitri, M. T.; Kelly, L.; Zhao, H.; Ichiyama, T.; Catania, A. α-MSH and Its Receptors in Regulation of Tumor Necrosis Factor-α Production by Human Monocyte/Macrophages. *Am. J. Physiol.* **1999**, *276*, 128–194.

39. Getting, S. J.; Gibbs, L.; Clark, A. J.; Flower, R. J.; Perretti, M. POMC Gene-Derived Peptides Activate Melanocortin Type 3 Receptor on Murine Macrophages, Suppress Cytokine Release, and Inhibit Neutrophil Migration in Acute Experimental Inflammation. *J. Immunol.* **1999**, *162*, 7446–7453.

40. Bohm, M.; Luger, T. A. Melanocortins in Fibroblast Biology—Current Update and Future Perspective for Dermatology. *Exp Dermatol.* **2004**, *13*, 16–21.

41. Caruso, F.; Caruso, R. A.; Mohwald, H. Nanoengineering of Inorganic and Hybrid Hollow Spheres by Colloidal Templating. *Science* **1998**, *282*, 111–114.

42. Ho, P. K.; Kim, J. S.; Burroughes, J. H.; Becker, B.; Li, J. F.; Brown, T. M.; Caciallin, F.; Friend, R. H. Molecular-Scale Interface Engineering for Polymer Light-Emitting Diodes. *Nature* **2000**, *404*, 481–484.

43. Hiller, J.; Mendelsohn, J. D.; Rubner, M. F. Reversibly Erasable Nanoporous Anti-reflection Coatings from Polyelectrolyte Multilayers. *Nat. Mater.* **2002**, *1*, 59–63.

44. Tang, Z.; Kotov, N. A.; Magonovand, S.; Ozturk, B. Nanostructured Artificial Nacre. *Nat. Mater.* **2003**, *2*, 413–418.

45. Jessel, N.; Atalar, F.; Lavalle, Ph.; Mutterer, J.; Decher, G.; Schaaf, P.; Voegel, J. C.; Ogier, J. Bioactive Coatings Based on Polyelectrolyte Multilayer Architecture Functionalized by Embedded Proteins. *Adv. Mater.* **2003**, *15*, 692–695.

46. Jessel, N.; Schwinte, P.; Donohue, R.; Lavalle, Ph.; Boulmedais, F.; Darcy, R.; Szalontai, B.; Voegel, J. C.; Ogier, J. Pyridylamino-β-Cyclodextrin as a Molecular Chaperone for Lipopolysaccharide Embedded in a Multilayered Polyelectrolyte. *Adv. Funct. Mater.* **2004**, *14*, 963–969.

47. Jessel, N.; Lavalle, Ph.; Hübsch, E.; Holl, V.; Senger, B.; Haïkel, Y.; Voegel, J. C.; Ogier, J.; Schaaf, P. Short-Time Tuning of the Biological Activity of Functionalized Polyelectrolyte Multilayer. *Adv. Funct. Mater.* **2005**, *15*, 648–654.

48. Picart, C.; Schneider, A.; Etienne, O.; Mutterer, J.; Schaaf, P.; Jessel, N.; Voegel, J. C. *In Vitro* and *In Vivo* Controlled Degradability of Polysaccharide Multilayer Films *In Vitro* and *In Vivo*. *Adv. Funct. Mater.* **2005**, *15*, 1771–1780.

49. Gangloff, S. C.; Ladam, G.; Dupray, V.; Fukase, K.; Brandenburg, K.; Guenounou, M.; Schaaf, P.; Voegel, J. C.; Jessel, N. Biologically Active Lipid an Antagonist Embedded in a Multilayered Polyelectrolyte Architecture. *Biomaterials* **2005**, *27*, 1771–1777.

50. Chu, S. C.; Tsai, C. H.; Yang, S. F.; Huang, F. M.; Su, Y. F.; Hsieh, Y. S.; Chang, Y. C. Induction of Vascular Endothelial Growth Factor Gene Expression by Proinflammatory Cytokines in Human Pulp and Gingival Fibroblasts. *J. Endod.* **2004**, *30*, 704–707.

51. Min, K. S.; Kwon, Y. Y.; Lee, H. J.; Lee, S. K.; Kang, K. H.; Lee, S. K.; Kim, E. C. Effects of Proinflammatory Cytokines on the Expression of Mineralization Markers and Heme Oxygenase-1 in Human Pulp Cells. *J. Endod.* **2006**, *32*, 39–43.

52. Tokuda, M.; Nagaoka, S.; Torii, M. Interleukin-10 Inhibits Expression of Interleukin-6 and -8 mRNA in Human Dental Pulp Cell Cultures *via* Nuclear Factor-κB Deactivation. *J. Endod.* **2002**, *28*, 177–180.

53. Silva, A. C.; Faria, M. R.; Fontes, A.; Campos, M. S.;

Cavalcanti, B. N. Interleukin-1β and Interleukin-8 in Healthy and Inflamed Dental Pulps. *J. Appl. Oral Sci.* **2009**, *17*, 527–532.

54. Yamamoto, M.; Sato, S.; Hemmi, H.; Uematsu, S.; Hoshino, K.; Kaisho, T.; Takeuchi, O.; Takeda, K.; Akira, S. TRAM Is Specifically Involved in the Toll-like Receptor 4-Mediated MyD88-Independent Signaling Pathway. *Nat. Immunol.* **2003**, *4*, 1144–1150.

55. O'Neill, L. A. TLRs: Professor Mechnikov, Sit on Your Hat. *Trends Immunol.* **2004**, *25*, 687–693.

56. Getting, S. J.; Schioth, H. B.; Perretti, M. Dissection of the Anti-inflammatory Effect of the Core and C-Terminal (KPV) α-Melanocyte-Stimulating Hormone Peptides. *J. Pharmacol. Exp. Ther.* **2003**, *306*, 631–635.

57. Murray, P. E.; Garcia-Godoy, F.; Hargreaves, K. Regenerative Endodontics: A Review of Current Status and a Call for Action. *J. Endod.* **2007**, *33*, 77–90.